# Antimicrobial 3D Porous Scaffolds Prepared by Additive Manufacturing and Breath Figures

Nelson Vargas-Alfredo,[1] Ane Dorronsoro,[2] Aitziber L. Cortajarena[2,3] and Juan Rodríguez-Hernández[1]*

1. Instituto de Ciencia y Tecnología de Polímeros (ICTP), Consejo Superior de Investigaciones Científicas (CSIC), C/Juan de la Cierva 3, 28006 Madrid, Spain. Email: jrodriguez@ictp.csic.es .

2. CIC biomaGUNE, Parque Tecnológico de San Sebastián, Paseo Miramón 182, 20014 Donostia-San Sebastián, Spain

3. Ikerbasque, Basque Foundation for Science, Mª Díaz de Haro 3, 48013 Bilbao, Spain

## Abstract

We describe herein a novel strategy for the fabrication of efficient 3D printed antibacterial scaffolds. For this purpose, both the surface topography as well as the chemical composition of 3D scaffolds fabricated by additive manufacturing were modified. The scaffolds were fabricated by fused deposition modeling (FDM) using high impact polystyrene (HIPS) filaments. The surface of the objects was then topographically modified providing materials with porous surfaces by means of the Breath Figures approach. The strategy involves the immersion of the scaffold in a polymer solution during a precise period of time. This approach permitted the modification of the pore size varying the immersion time as well as the solution concentration. Moreover, by using polymer blend solutions of polystyrene and polystyrene-*b*-poly(acrylic acid) ($PS_{23}$-*b*-$PAA_{18}$) and a quaternized polystyrene-*b*-poly(dimethylaminoethyl methacrylate) ($PS_{42}$-*b*-$PDMAEMAQ_{17}$), the scaffolds were simultaneously chemically modified. The surfaces were characterized by scanning electron microscopy and FT-IR. Finally, the biological response towards bacteria was explored. Porous surfaces prepared using quaternized PDMAEMA as well as those prepared using PAA confer antimicrobial activity to the films, *i.e.* were able to kill on contact *S. aureus* employed as model bacteria.

**Keywords**

Antibacterial polymer surfaces, cell adhesion, additive manufacturing, Breath Figures, chemical surface treatment, fused deposition modeling, porous surface

## Introduction

Biomedical devices are today widely employed and are a crucial aspect of the human healthcare system. For instance, the use of knee implants or artificial hips and has continuously increased during the last decades. Equally, vascular grafts, heart valves, and stents are currently widely used both to save lives and to restore the quality of life for many patients. Within this context, polymers is probably the fastest growing category among all segments during 2013 to 2019[1]. Several advantages in the use of polymers including flexibility, elasticity, biocompatibility, bio-inertness in comparison to metal counterparts have made of these materials excellent candidates for biomedical purposes. Nevertheless, an important issue in the use of polymeric materials applications for biorelated purposes still remain unresolved and concerns the material contamination by different microorganisms present in the environment and in particular by bacteria. This problem affects not only different areas as medical devices, healthcare products but it is also crucial in the fabrication of water purification systems, dental office equipment, food packaging, food storage or household sanitation.[2]

Current strategies to fabricate antimicrobial materials are typically based on the immobilization of synthetic killing substances onto materials' surfaces. However, most of these approaches presented either incomplete efficiency, eventually toxicity or can play an important role in the emergence of multiresistant bacteria.[3] To the best of our knowledge, at the present, there is not a single strategy that could totally eliminate the incidence of infections associated to biomaterials.[4]. A large number of studies have explored the surface chemical modification of polymeric materials and today a general agreement has been obtained. Although chemically based bactericidal mechanisms are known to be effective, both the duration and specificity of any particular chemical antibacterial mechanism need to be improved. Equally, the duration of the antimicrobial activity still remain limited. In addition to the surface chemical modification, great consideration is currently being given to explore the role that the surface topography plays

in the antibacterial/antibiofouling properties of surfaces particularly at the micro/nanoscale.[5] In effect, the micro/nano surface topographical features have a clear influence on the microorganism adhesion [6-17] but may also act as antimicrobials by physically disrupting the bacterial membrane. [18] Most of the works reported up to date have focused on the fabrication of planar films having micro or nanotopographical features and, in the most sophisticated cases, having a particular surface chemical composition. However, there is no precedent in the fabrication of intricate 3D geometries with antimicrobial/antifouling properties.

The fabrication of polymeric 3D objects with intricate shapes is today accessible thanks to the advances in novel fabrication technologies, but especially to the development of alternative fabrication methodologies such as additive manufacturing (AM).[19-22] Additive manufacturing, also known as free-form fabrication or rapid prototyping allows for the preparation of 3D parts and objects. This fabrication methodology is based on computer designs that allow us to easily modulate both the shape and dimensions of the object. The resolution as well as the object dimension has been significantly improved and today it is possible to prepare fully customized parts with micrometer resolution and decimeters in size. As a result, 3D printing is today one of the most relevant next-generation manufacturing methodologies, for instance, in the design and fabrication of devices, in particular, for biomedical applications.[23, 24] 3D printing is currently evaluated for the fabrication of many different scaffolds for tissue engineering [21, 25], bone regeneration [22, 26, 27] or to create dental models [19] and organs that can help in the elaboration of surgical plans.[28, 29]

In this manuscript, we propose a strategy that takes advantage of the use of high impact polystyrene (HIPS) (a widely employed commodity polymer) and 3D printing to create 3D objects and modify, independently of the explored geometry, both surface topography and chemical composition. In particular, the breath figures (BFs) approach has been carried out using polymer blends comprising a polymer matrix and functional block copolymers to provide 3D objects with variable surface chemical composition. As a proof of concept, the surface modification (topographically and chemically) on different scaffolds will be described.[27]

Breath figures will enable the formation of porous surfaces by evaporation of a polymer solution in a moist atmosphere. While, several methodologies have been employed including solvent casting, spin coating or dip coating to fabricate planar porous surfaces [30-36], examples about the preparation of non-planar surfaces are scarce.[37-40] Moreover, to the best of our knowledge there is no precedent in the fabrication of breath figures at the surface of complex geometries obtained by additive manufacturing.

## Experimental section

### Materials

Styrene (St) (Sigma, Aldrich, 99 %) and *t*-butyl acrylate (tBA) (Sigma-Aldrich, 98 %) were distilled under reduced pressure over calcium hydride prior to use. Copper (I) bromide (CuBr) (Sigma-Aldrich, 98%), 2,2'-bipyridyl (bipy) (Sigma-Aldrich, 99 %), N,N,N',N'',N''',-pentamethyldiethylenetriamine (PMDETA) (Sigma-Aldrich, 99 %), phenylethyl bromide (PhEBr) (Sigma-Aldrich, 97 %), and other solvents were used as received. The diblock copolymers were prepared by atom-transfer radical polymerization (ATRP) in two steps following previously reported procedures [39].

Polystyrene filaments were purchased from Impresoras 3D (ESUN HIPS). According to the supplier contains around 85 wt% of PS, 10 wt% acrylonitrile and 5 wt% butadiene. High molecular weight polystyrene (Aldrich, $M_w$ =2.50·$10^5$ g/mol) was used as polymeric matrix. Chloroform ($CHCl_3$) was purchased from Scharlau.

### Characterization

ATR-FTIR measurements are carried out using an FTIR spectrometer Spectrum One of Perkin-Elmer equipped with a single reflection ATR device using as internal reflection elements diamond/ZnSe. This setup allows for studying the samples with a penetration depth of around 2 μm. To determine the modification of the 3D printed objects, the band 2850 $cm^{-1}$ was used that

correspond to the polymeric main chains of PS and compared with characteristic signals of the different functional polymers. In the case of PAA and PDMAEMA present a characteristic peak at ~1720 $cm^{-1}$ due to carbonyl group of the methacrylate.

Scanning electron microscopy (SEM) micrographs were taken using a Philips XL30 with an acceleration voltage of 25 kV. The samples were coated with gold-palladium (80/20) prior to scanning. The analysis of the pore size (average diameter) and pore size distribution were performed using the image analysis software (ImageJ, http://rsb.info.nih.gov/ij/).

ATR-FTIR measurements are carried out using an FTIR spectrometer Spectrum One of Perkin-Elmer equipped with a single reflection ATR device using as internal reflection elements diamond/ZnSe. This setup allows for studying the samples with a penetration depth of around 2 μm.

**Synthesis of the functional block copolymers**

**Synthesis of polystyrene macroinitiator (PS-Br)**

In a typical polymerization experiment, 0.60 g (3.2 mmol) phenylethyl bromide, 0.56 g (3.2 mmol) N,N,N',N'',N''-pentamethyldiethylenetriamine and 0.46 g (3.2 mmol) CuBr were placed in a dried 100 ml three-necked flask which was flushed with nitrogen. Pre-degassed styrene (20 g, 192 mmol) was added to the flask immersed in an oil bath at 85°C, and then the solution was magnetically stirred for 4 h under a nitrogen atmosphere. Over this period the originally red translucent polymeric solution turned dark and opaque. After the polymerization was completed, the polymer was diluted by 20 ml $CHCl_3$, and then precipitated in excess methanol after passing through an alumina column. The white powder was purified by re-dissolution in $CHCl_3$ and reprecipitation in methanol, and then dried at 60°C under vacuum.

**Synthesis of polystyrene-block-poly(acrylic acid) ($PS_n$-*b*-$PtBA_m$)**

The macroinitiator PS-Br and 5 mL of degassed acetone were added to the mixture ([M]:[I]:[CuBr]:[L] = 400:1:1:1). Acetone enhanced the solubility of the CuBr/PMDETA

complex. The polymerization of tert-butyl acrylate (tBA) was carried out at 65 °C. The copolymer composition was determined by $^1$H-NMR to be $PS_{23}$-*b*-$PAA_{18}$.

**Hydrolysis of the PtBA block in the $PS_n$-*b*-$PtBA_m$.**

Copolymers were first dissolved in $CH_2Cl_2$. Trifluoroacetic acid (TFA) was then added (10 equivalents to tert-butyl ester units), and the mixture was stirred at room temperature for 3 days. The deprotected polymers, precipitated in the reaction media, were filtered and washed with $CH_2Cl_2$ and finally dried under vacuum.

**Synthesis of polystyrene-block-poly(dimethylaminoethyl methacrylate) ($PS_n$-b-$PDMAEMA_m$)**

Synthesis of block copolymer: In a Schlenk tube, 0.819 g (0.182 mmol) PS-Br macroinitiator, 0.019 g (0.135 mmol) CuBr, and 0.023 g (0.135 mmol) N,N,N',N'',N''-pentamethyldiethylenetriamine (PMDETA), 20 ml of pre-degassed DMF was introduced under nitrogen atmosphere. The Schlenk was immersed in an oil bath at 90°C and the ATRP was started by adding 2.55 g (16.2 mmol) of DMAEMA. The reaction was left for 24 h with continuous stirring. After the polymerization was completed, the former block was precipitated in methanol after passing through an alumina column, and dried at 60°C under vacuum. According to $^1$H-NMR the block copolymer has a composition of $PS_{42}$-*b*-$PDMAEMA_{17}$. GPC of the block copolymers carried out in THF evidenced narrow polydispersity between 1.22-1.26 evidencing a complete initiation of the polystyrene macroinitiator.

**Quaternization of the PDMAEMA units in the block copolymers**

In a round bottom flask was introduced 0.1g ($2.33x10^{-4}$ mol of tertiary amine groups) of block copolymer $PS_{42}$-*b*-$PDMAEMA_{17}$ and dissolved in 1.0 ml of THF under stirring at room temperature. Next, 0.0661g ($4.65x10^{-4}$ mol) of $CH_3I$ was added. After 20h, the quaternized

copolymer was observed in form of a white powder precipitate. After evaporation of the solvent and residual $CH_3I$ a white powder was recovered and analyzed by $^1$H-NMR.

**Fabrication of the 3D printed parts via FDM**

Designs were created using the 3D CAD program Autodesk Inventor 2015. The 3D printed objects were fabricated using an Anet A3 printer using a commercially available 1.75mm diameter polystyrene filament. Cura 3D Printing Slicing Software was employed to calculate the noozle pathway. The temperature employed to melt and deposit the material was set to 258ºC and the z-step fixed to 200μm.

**Preparation of the porous surfaces by the Breath Figures approach**

The Breath Figures approach was employed to produce porous surfaces on the 3D printed objects. For that purpose, the objects were submerged into a chloroform solution containing a variable concentration of high molecular weight polystyrene (0-30mg/ml) and five different copolymers, i.e. polystyrene-*b*-poly(acrylic acid) ($PS_{23}$-*b*-$PAA_{18}$), polystyrene-*b*-poly(dimethylaminoethyl methacrylate) ($PS_{42}$-*b*-$PDMAEMA_{17}$), a quaternized polystyrene-*b*-poly(dimethylaminoethyl methacrylate) ($PS_{42}$-*b*-$PDMAEMAQ_{17}$). The immersion time was equally varied during 1, 3 and 5 seconds. The process was carried out inside a closed chamber with saturated relative humidity (RH) at room temperature.

**Bacterial adhesion and live/dead assays**

*Staphylococcus aureus* strain RN4220 carrying the plasmid pCN57 for green fluorescent protein (GFP) expression was grown overnight at 37°C in Luria–Bertani (LB) media with erythromycin (10 μg $mL^{-1}$). The cells were centrifuged and washed three times in PBS saline buffer (150 mM NaCl phosphate 50 mM, pH 7.4). The solution was adjusted to a cell concentration that corresponds to an optical density (OD) at 600 nm of 1.0 corresponding to approximately 1.5 $10^9$ colony forming units (CFU)/ml.

The different patterned polymeric surfaces were incubated for 1 hour with bacterial suspensions in PBS at OD = 1.0. After incubation the surfaces were washed with PBS buffer three times for 15 minutes. After washing, bacterial adhesion was monitored by fluorescence microscopy using a Leica DMI-6000 fluorescence microscope. Images were acquired using a x63 magnification objective and the corresponding set of filter for imaging green fluorescence corresponding to the GFP expressed in the bacteria.

After adhesion, the bacteria viability was measured using Propidium iodine staining, as indicated in the LIVE/DEAD BacLight Bacterial Viability Kit. Propidium iodine is a red-fluorescent nucleic acid stain that penetrates only cells with disrupted membranes and intercalates DNA. The different surfaces with attached bacteria were incubated with propidium iodide (5 mg $mL^{-1}$) for 15 minutes, followed by rinsing with PBS solution (10 times). Phase contrast, green and red fluorescence microscopy images were taken at x63 magnification. The number of total bacteria is quantified from the green bacteria, and the dead bacteria are stained also in red. The bacterial cell density and the viability were quantified from the microscopy images using ImageJ.

**Results and Discussion**

**Fabrication of 3D printed parts based on PS**

Fused deposition modeling (FDM) was employed as a free-form fabrication methodology to manufacture 3D objects. The HIPS filament was directly deposited layer by layer by melting the polymer through a 400 μm nozzle. The low cost of this alternative for 3D fabrication is one of the major advantages of this methodology that with a resolution of hundreds of microns is useful for 3D objects with centimeter/decimeter sizes. As depicted in **Figure 1 (a)-(d)**, for this study we prepared four different 3D structures with variable cylinder geometries. The z-resolution was fixed to 200 μm.

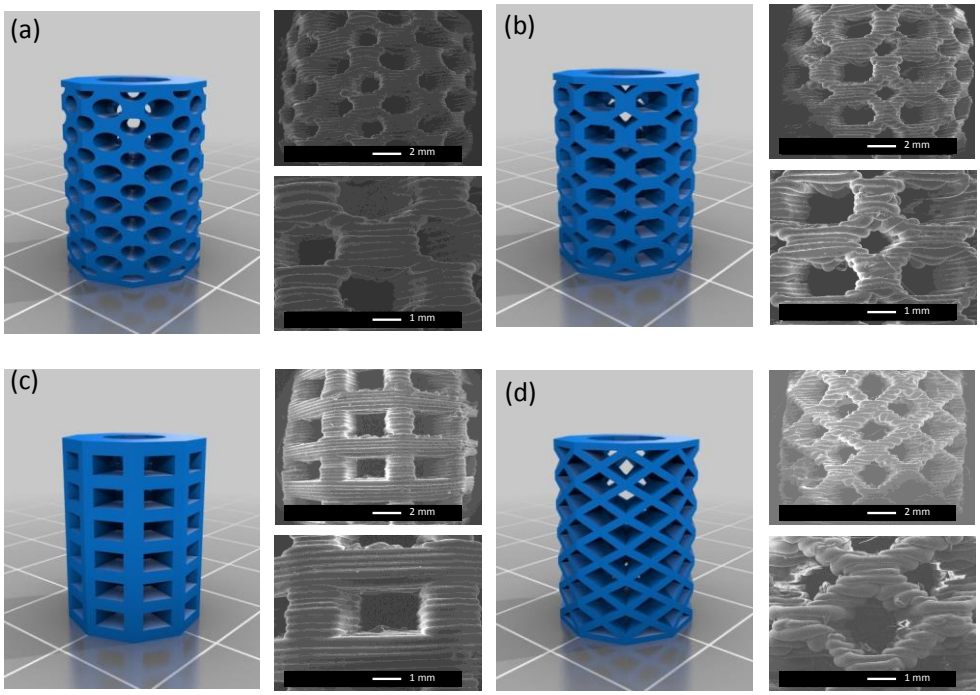


**Figure 1.** Models and the corresponding SEM images of the 3D printed parts employed in this study. We explored the surface modification (topographically and chemically) with antimicrobial moieties on different scaffolds with variable geometries.

The strategy proposed herein to fabricate either antifouling or selective antimicrobial surfaces is based on the surface functionalization of the 3D printed parts by simultaneously changing the topography at the micrometer scale and introducing different antimicrobial functional groups at the surface. Provided this precise functionalization, we hypothesize, based on our previous findings [41], that bacteria (having dimensions ranging from 1 μm and even below (e.g. *S. aureus*) up to 5 μm in the case of *Escherichia coli*) will be able to enter in the micrometer size pores. As a result, bacteria are expected to be killed upon contact with the antimicrobial functional groups placed at the pore wall.

The chemical structures of the polymers employed are depicted in **Figure 2**. Polystyrene (1) will be the main component of the blends and is identical to the material employed to fabricate the 3D objects. The functional copolymers employed in this study are block copolymers have

been prepared to decorate the surfaces with antimicrobial moieties. On the one hand, polystyrene-*b*-poly(acrylic acid) ($PS_{23}$-*b*-$PAA_{18}$), bearing negatively charged acrylic acid groups recently reported as potent antimicrobial polymer [42] will be explored. On the other hand, polystyrene-*b*-poly(dimethylaminoethyl methacrylate) ($PS_{42}$-*b*-$PDMAEMA_{17}$), that upon quaternization (quaternized polystyrene-*b*-poly(dimethylaminoethyl methacrylate) ($PS_{42}$-b-$PDMAEMAQ_{17}$) provide quaternary ammonium salts that have equally exhibited excellent antimicrobial response.[43]

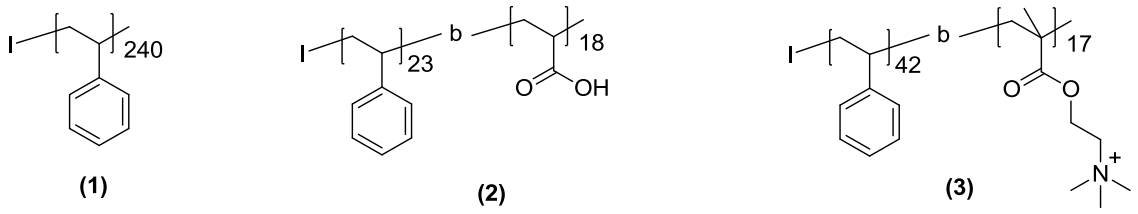


**Figure 2.** Scheme of the copolymers employed for the functionalization of 3D printed parts (1) polystyrene employed as polymer matrix, (2) polystyrene-*b*-poly(acrylic acid) ($PS_{23}$-*b*-$PAA_{18}$) and (3) polystyrene-b-poly(dimethylaminoethyl methacrylate quaternized) ($PS_{42}$-*b*-$PDMAEMAQ_{17}$),

The preparation of the functional porous surfaces on the 3D objects by using the Breath Figures approach was carried out in one single step as is schematically shown in **Figure 3**. The BFs methodology enables the formation of pores upon simultaneous solvent evaporation from a polymer solution and water droplet condensation at the solvent/air interface occurring in a moist atmosphere.[44-46] The 3D printed parts were immersed in a polymer solution that contains the polymer matrix (i.e. high molecular weight polystyrene) and a variable amount of the block copolymers. As depicted in **Figure 3**, the objects (a) were submerged for 1-5 seconds in a polymer blend solution using chloroform as solvent (b). During these short periods of time, the polymer solution forms a thin coating at the surface of the object (c) that, upon evaporation of the solvent, leaves a thin layer of the polymer blend over the entire surface of the 3D object.

More interestingly, when the evaporation is carried out in a moist atmosphere, water vapor condenses at the surface (d) forming water droplets that finally evaporate and produce micrometer size pores (e). As evidenced in **Figure 3,** the initial, 3D printed part exhibit a rough but planar surface that upon Breath Figures formation changed into a porous surface. Interestingly, this methodology permits the formation of pores over the entire surface independently of the geometry of the 3D object which supposes a clear advantage over other surface patterning techniques.

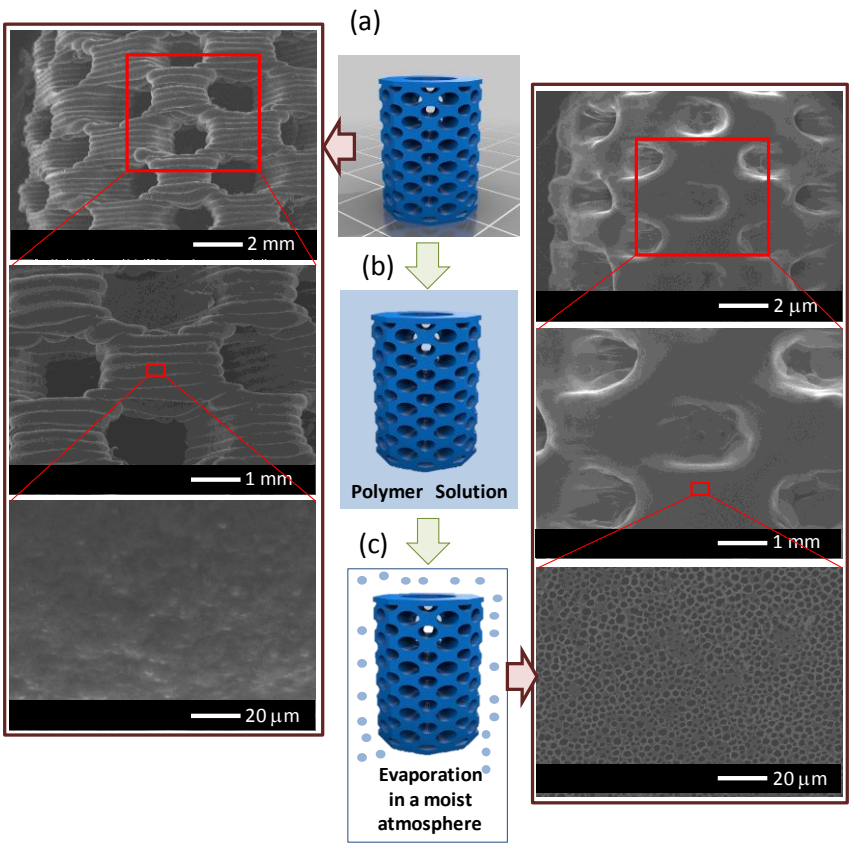


**Figure 3.** Scheme of the fabrication of functional porous surfaces on a 3D printed scaffold by using the breath Figures approach. (a) 3D model of the printed part and SEM images of the original surface topography. The scaffold was immersed in a polymeric solution (comprising PS and any of the block copolymers) with variable concentration 5-30 mg/ml) during 1-5 seconds (b). A thin polymer layer coats the material interface. The solvent evaporation is carried out in a moist atmosphere and water vapor condenses at the surfaces forming water droplets (c). Finally, the evaporation of the condensed water droplets finally produces the formation of porous

surfaces (e). On the right side, are included the SEM images after breath figures formation evidencing the formation of micrometer size pores at the surfaces of the 3D printed part. In this case, the scaffold was immersed in a 5mg/ml of PS/$PS_{23}$-*b*-$PAA_{18}$ chloroform solution during 1 second.

This simple strategy needs, however, of an optimization of the experimental conditions. Several parameters including relative humidity, polymer concentration or even blend composition have been demonstrated to play a crucial role on the size and homogeneity of the pores formed at the surface. Herein, based on previous works carried out on planar films, we have maintained constant the relative humidity at 99% and the blend composition to 20% of block copolymer and 80% of polymer matrix while both the polymer concentrations as well as the immersion time were varied in order to explore the formation of the porous interfaces.

The first series of experiments were carried out maintaining the polymer concentration 30 mg/ml and varying the immersion time (1, 3 and 5s). In **Figure 4** are presented the microscopy images of the films prepared using either $PS_{23}$-*b*-$PAA_{18}$ or $PS_{42}$-*b*-$PDMAEMA_{47}$. From the images presented in **Figure 4** and **Figure 5**, it can be concluded that by increasing the immersion time surfaces with larger pores were obtained. For instance, in Figure 4(a) are included the microscopy images of the porous surfaces prepared using PS/PS-b-PAA blends for the three immersion times selected, i.e. 1, 3 and 5s. Whereas, average pore sizes around 3.7 μm were obtained for 1 s immersion, pores with pore sizes around 4.5 μm were measured for 5 seconds immersion time. It is worth mentioning that larger immersion times produced rough surfaces with uncontrolled pore sizes. In effect, larger immersion starts to dissolve the HIPS and the surface topography is significantly affected by this process.

In addition of the immersion time, the pore size is also directly related to the polymer concentration in the solution. In order to analyze this parameter, coatings using polymer solutions with concentrations ranging between 5 and 30 mg/ml were prepared. In **Figure 4** are

depicted the SEM images obtained for each concentration using either a blend composed of 80% of PS and 20% of $PS_{23}$-*b*-$PAA_{18}$ a blend composed of 80% of PS and 20% of $PS_{42}$-*b*-$PDMAEAMA_{17}$. Films prepared using lower concentrations (*i.e.* 5mg/ml and 10 mg/ml) lead, in general, to more heterogeneous surfaces and larger pores most probably due to the partial coagulation between condensed water droplets. The use of higher concentrations (30mg/ml) polymer solutions slightly improved the order of the pores and simultaneously produced surfaces with lower average pore sizes. As shown in **Figure 5**, an increase of the polymer concentration can produce surfaces with average pore sizes around 2-3 μm smaller.

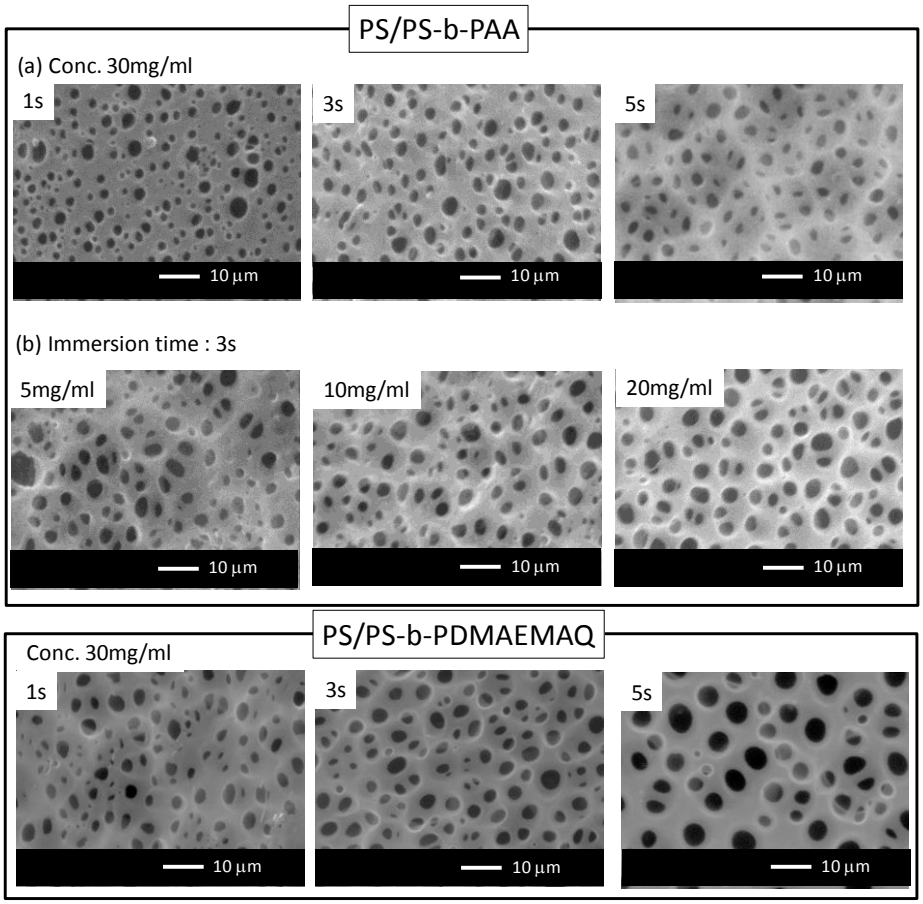


**Figure 4.** Influence of the immersion time and polymer concentration on the pore size. The porous surfaces were obtained by immersion of the 3D printed part in a polymer solution formed by 80% of PS and 20% of $PS_{23}$-*b*-$PAA_{18}$. The relative humidity employed is around 99%. (a) Variation of the immersion time for a sample prepared from polymer solutions at 30mg/ml (b) Immersion time fixed to 5s and concentrations varied between 5 and 20mg/ml.

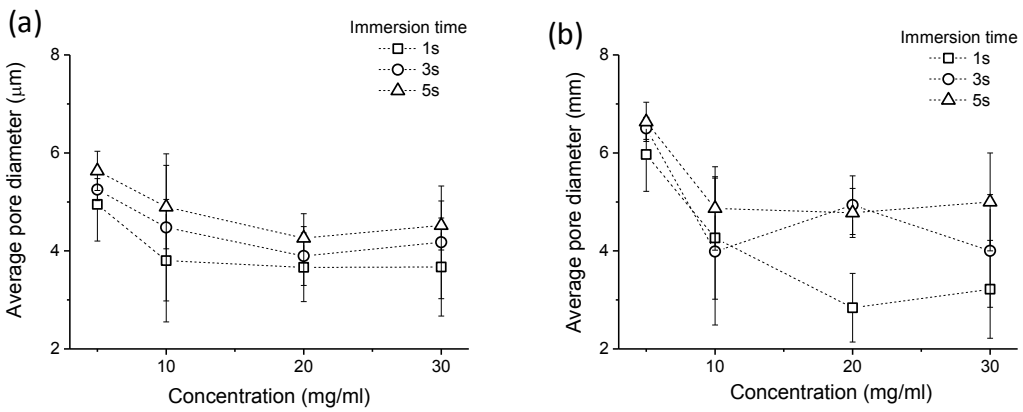


**Figure 5.** Variation of the average pore size at the surface of the 3D printed parts as a function of the polymer concentration for the three immersion times explored, i.e. 1, 3 and 5s. The relative humidity was maintained at 99%. Left: 3D parts functionalized with a polymer blend composed of 20% $PS_{23}$-*b*-$PAA_{18}$/80% PS. Right: 3D parts functionalized with a polymer blend composed of 20% $PS_{42}$-*b*-$PDMAEMA_{17}$/80% PS.

As has been mentioned, in addition to the pore size, the strategy proposed using polymer blends permit to vary the surface chemical composition by using the appropriated functional copolymer. The surface chemical composition of the systems explored herein was analyzed by FT-IR. Illustrative spectra for the 3D printed parts modified with a blend of 20% $PS_{42}$-*b*-$PDMAEMA_{17}$/80% PS are depicted in **Figure 6(a)**. For comparative purposes, the FT-IR spectra of the surface of a 3D printed and non-treated object has been equally included. A relatively low intensity signal of the -C=O group present in the 3D printed can be observed indicating that a slight oxidation of the HIPS is produced during the melting and printing process. Nevertheless, the intensity of the –C=O group signal is present and even increases gradually with the concentration of the polymer solution employed. On the one hand, this signal was observed in the different areas of the 3D printed part (error bars are included in the graph) indicating the formation of a rather homogeneous coating and the presence of the functional groups at the surface of the object. On the other hand, it has to be clarified that this increase in intensity is not due to a larger amount of PDMAEMA at the interface since the composition of

the polymer solution was maintained constant but to the deposition of a thicker polymer layer at the surface of the 3D printed part. In effect, thinner layers are expected for coatings prepared using diluted polymer concentrations. Therefore, a larger contribution of the HIPS versus the polymer blend is attended. On the contrary, those coatings prepared using larger polymer concentrations form thicker polymer blend layers and therefore the relative signal of the -C=O groups of the diblock copolymer increased. A similar behavior was observed for both systems as depicted in **Figure 6(b)** where are represented the intensities of the C=O signal versus the aromatic signal provided by the PS. In all cases, an increase of the relative intensity of the carbonyl signal indicates the formation of a thicker layer of the polymer blend at the surface of the object.

(a)

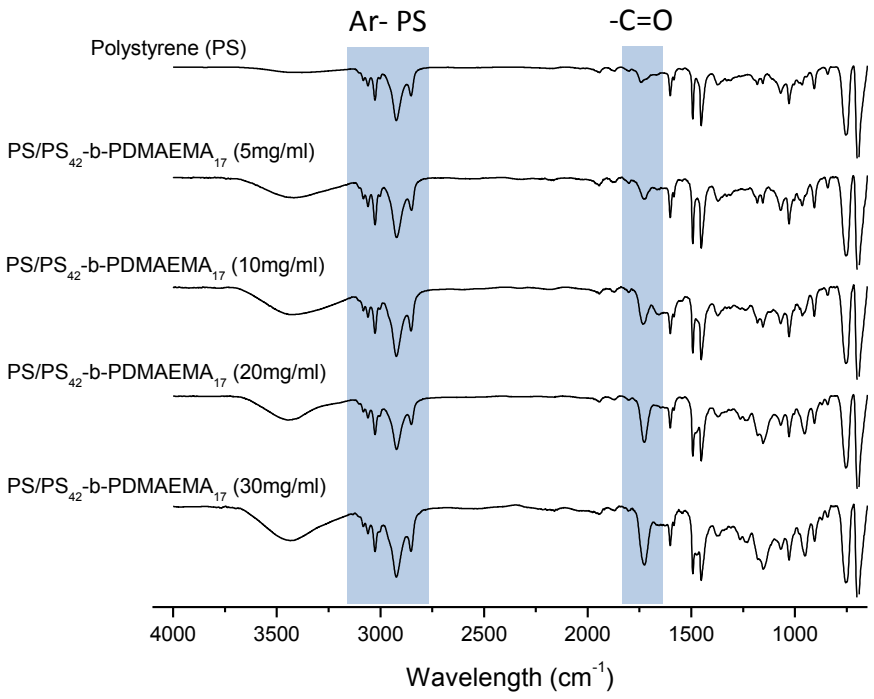


(b)

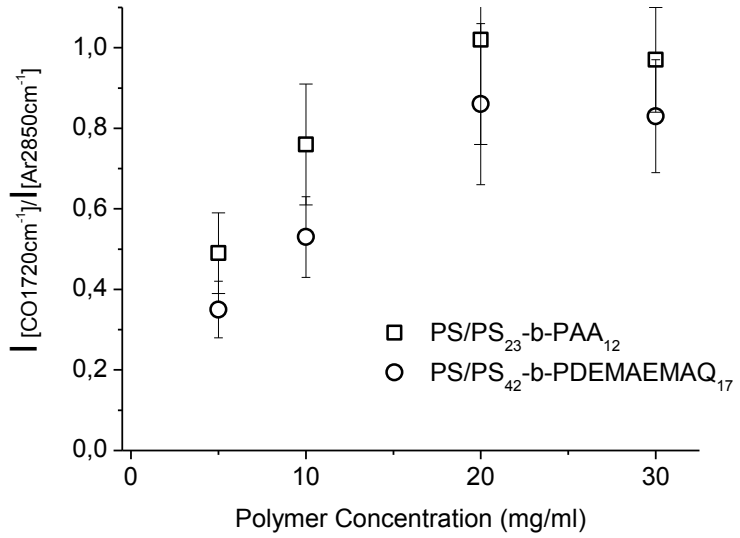


**Figure 6.** (a) Illustrative FT-IR spectra of the 3D printed parts functionalized by using a polymer solution of PS and $PS_{42}$-*b*-$PDMAEMA_{17}$ with variable polymer concentration. (b) Variation of the relative intensity of the C=O signal at 1720$cm^{-1}$ versus the aromatic signal at 2850 $cm^{-1}$ as a function of the polymer concentration. The –C=O signal, provided either by PAA or PDMAEMA can be employed to explore the variation of the presence of these two block copolymers at the surface. The immersion time was 1s.

Provided the surface functionalization and the surface topography with control over the average pore diameter, both the bacterial adhesion properties and the antibacterial activity of the surfaces were tested following previously established protocols [47]. For this study, *S. aureus* was used as model bacteria since it is a common pathogen responsible of many hospital-acquired infections, through a strain that has acquired resistance to antibiotics (Methicillin-resistant *Staphylococcus aureus*, MRSA) and also of many common skin infections. Two functionalized surfaces were selected to evaluate the antibacterial performance prepared by immersing the objects in a polymer blend solution during 1s and using a polymer concentration of 30 mg/ml. The surfaces were incubated with standardized solution of green fluorescent *S. aureus*, washed and imaged using a fluorescence microscope to determine the adhesion of the

bacteria on the surfaces. The quantification of the number of bacteria per surface area upon 1 h incubation shows similar adhesion to all the surfaces including the control polystyrene surface.

After the adhesion studies, the bactericidal activity of the surfaces was evaluated and the effect of the functionalization with PDMAEMAQ and PAA was compared to the effect of the control PS surfaces. The bactericidal properties were measured by staining of the adhered bacteria with a red fluorescent dye that only penetrates permeabilized (i.e. died) cells right after the adhesion, 24, and 48 hours after. Fluorescent images are acquired in order to calculate percentage of live and dead bacteria under each experimental condition. The values obtained are represented in **Figure 8**. As expected, the PS control did not show bactericidal activity over time. However, introducing either PAA of PDMAEMAQ in the composition significantly improved the bactericidal properties of the surfaces. PAA containing diblock copolymers have been previously reported to kill bacteria and prevent from biofilm formation[42], in agreement with our results. A quantification of the bactericidal activity was obtained from the fluorescence microscopy using Image J (**Figure 8**). The quantitative results for PS-*b*-PAA diblock copolymer show that after 24 hours incubation present full bactericidal activity with 100 % of the adhered bacteria being killed. The same protocol was followed for the surfaces prepared with PDMAEMAQ. Similarly to the previous case, an excellent antimicrobial activity has been observed even upon 24h of incubation. These results evidenced the excellent antimicrobial properties of the prepared surfaces with either negatively charged carboxylic acid groups or positively charge quaternary ammonium groups.

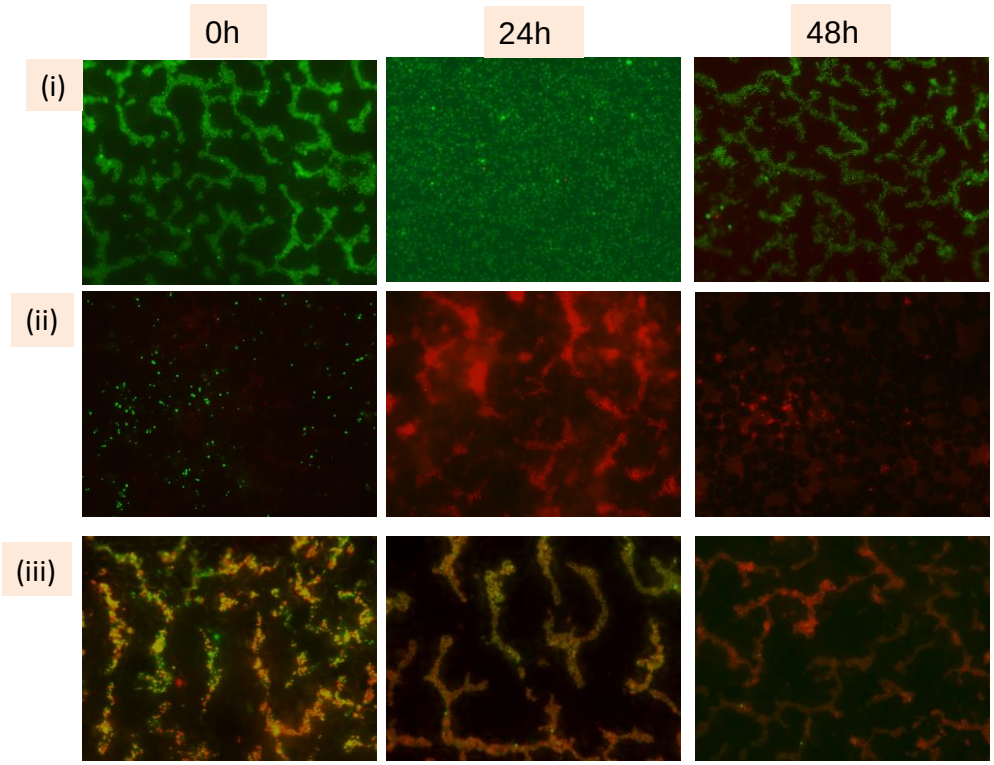


**Figure 7.** Evolution of the bacterial viability at different times 0, 24h and 48 h on porous surfaces prepared using (i) only polystyrene (ii) 20% $PS_{23}$-*b*-$PAA_{12}$/80% PS and (iii) 20% $PS_{42}$-*b*-$PDMAEMAQ_{17}$/80% PS, The fluorescence microscopy images show the polymeric surfaces incubated with *S. aureus* labeled with Green fluorescent protein and stained with propidium iodide (red). Images were acquired using the green and red channels at 63x magnification. For each polymeric surface overlay images of the two channels are generated using Image J. The scale bar corresponds to 20 μm.

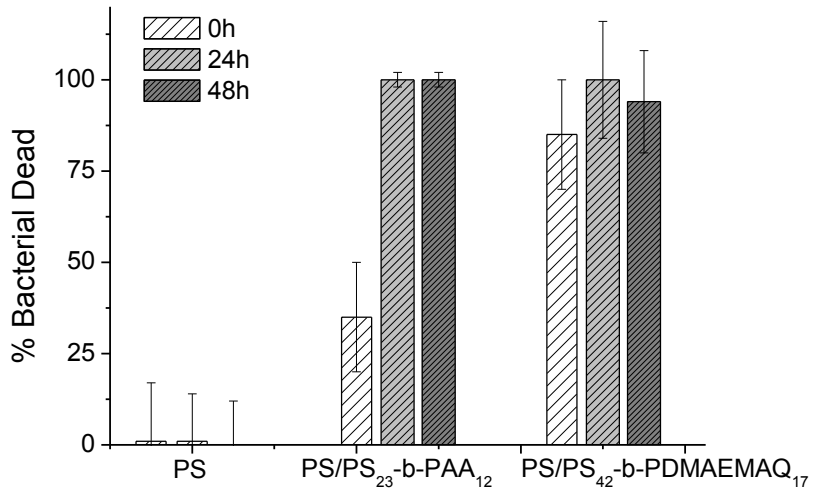


**Figure 8.** Quantification of the % of bacteria dead at different times 0, 24h and 48 h on the different porous surfaces tested. The quantification was performed by counting the number of cells stained in red or in green using Image J.

## Conclusions

We succeeded in the preparation of 3D printed PS objects with intricate geometries that were simultaneously functionalized and micropatterned at the surface in one single step. For this purpose, we employed the Breath Figures approach using polymer blend solutions to control simultaneously both functionality and topography. The strategy involves the dip coating of the 3D printed parts during periods of time ranging between 1 and 5 seconds in a polymer solution composed of polystyrene and an amphiphilic diblock copolymer. As a result of this process, a thin layer of the polymer solution coats the surface of the object that upon evaporation in a moist atmosphere and water vapor condensation leads to porous and functional surfaces.

Interestingly, the porous films fabricated with either PS-*b*-PAA or PS-b-PDMAEMA diblock copolymer display efficient bactericidal activity. It is worth mentioning that even when the exact mechanism of antibacterial activity needs further investigations, we can hypothesize that,

according to previous works, the pore sizes in the range of 1-1.5 μm would permit the immobilization of the bacteria. As a result, these are extensively killed due to the functional groups present in the pore cavity.

Current on-going work is devoted to the fabrication of antimicrobial porous surfaces and the evaluation of different parameters on the antimicrobial activity including the functional group density at the surface, the composition of the block copolymer as well as the role of the pore diameters.

**Acknowledgments**

The authors gratefully acknowledge support from the Consejo Superior de Investigaciones Científicas (CSIC). Equally, this work was financially supported by the Ministerio de Economía y Competitividad (MINECO) through MAT2016-78437-R, BIO2012-34835 and BIO2017-77367-C2-1R projects.

**References**

[1] I.M.D.t.I.M.R. Freedonia, Market Share, Market Size, Sales, Demand Forecast,, C.P. Market Leaders, Industry Trends, 2012, p. 395.
[2] E.-R. Kenawy, S.D. Worley, R. Broughton, The Chemistry and Applications of Antimicrobial Polymers: A State-of-the-Art Review, Biomacromolecules 8(5) (2007) 1359-1384.
[3] S.R. Shah, A.M. Tatara, R.N. D'Souza, A.G. Mikos, F.K. Kasper, Evolving strategies for preventing biofilm on implantable materials, Materials Today 16(5) (2013) 177-182.
[4] K. Glinel, P. Thebault, V. Humblot, C.M. Pradier, T. Jouenne, Antibacterial surfaces developed from bio-inspired approaches, Acta Biomaterialia 8(5) (2012) 1670-1684.
[5] K.A. Whitehead, J. Colligon, J. Verran, Retention of microbial cells in substratum surface features of micrometer and sub-micrometer dimensions, Colloids and Surfaces B: Biointerfaces 41(2–3) (2005) 129-138.
[6] M. Salta, J.A. Wharton, P. Stoodley, S.P. Dennington, L.R. Goodes, S. Werwinski, U. Mart, R.J.K. Wood, K.R. Stokes, Designing biomimetic antifouling surfaces, Philosophical Transactions of the Royal Society a-Mathematical Physical and Engineering Sciences 368(1929) (2010) 4729-4754.
[7] D.Y.C. Chan, M.H. Uddin, K.L. Cho, I.I. Liaw, R.N. Lamb, G.W. Stevens, F. Grieser, R.R. Dagastine, Silica nano-particle super-hydrophobic surfaces: the effects of surface morphology and trapped air pockets on hydrodynamic drainage forces, Faraday Discussions 143 (2009) 151-168.
[8] X.-M. Li, D. Reinhoudt, M. Crego-Calama, What do we need for a superhydrophobic surface? A review on the recent progress in the preparation of superhydrophobic surfaces, Chemical Society Reviews 36(8) (2007) 1350-1368.

[9] B. Bhushan, Y.C. Jung, Natural and biomimetic artificial surfaces for superhydrophobicity, self-cleaning, low adhesion, and drag reduction, Progress in Materials Science 56(1) (2011) 1-108.
[10] Y.Y. Yan, N. Gao, W. Barthlott, Mimicking natural superhydrophobic surfaces and grasping the wetting process: A review on recent progress in preparing superhydrophobic surfaces, Advances in Colloid and Interface Science 169(2) (2011) 80-105.
[11] K. Koch, W. Barthlott, Superhydrophobic and superhydrophilic plant surfaces: an inspiration for biomimetic materials, Philosophical Transactions of the Royal Society a-Mathematical Physical and Engineering Sciences 367(1893) (2009) 1487-1509.
[12] K. Koch, B. Bhushan, W. Barthlott, Multifunctional surface structures of plants: An inspiration for biomimetics, Progress in Materials Science 54(2) (2009) 137-178.
[13] K. Koch, H.F. Bohn, W. Barthlott, Hierarchically Sculptured Plant Surfaces and Superhydrophobicity, Langmuir 25(24) (2009) 14116-14120.
[14] A.J. Schulte, K. Koch, M. Spaeth, W. Barthlott, Biomimetic replicas: Transfer of complex architectures with different optical properties from plant surfaces onto technical materials, Acta Biomaterialia 5(6) (2009) 1848-1854.
[15] J.B. Boreyko, C.H. Baker, C.R. Poley, C.-H. Chen, Wetting and Dewetting Transitions on Hierarchical Superhydrophobic Surfaces, Langmuir 27(12) (2011) 7502-7509.
[16] N.J. Shirtcliffe, G. McHale, S. Atherton, M.I. Newton, An introduction to superhydrophobicity, Advances in Colloid and Interface Science 161(1-2) (2010) 124-138.
[17] C. Yang, U. Tartaglino, B.N.J. Persson, Influence of surface roughness on superhydrophobicity, Physical Review Letters 97(11) (2006).
[18] E.P. Ivanova, J. Hasan, H.K. Webb, T. Vi Khanh, G.S. Watson, J.A. Watson, V.A. Baulin, S. Pogodin, J.Y. Wang, M.J. Tobin, C. Loebbe, R.J. Crawford, Natural Bactericidal Surfaces: Mechanical Rupture of Pseudomonas aeruginosa Cells by Cicada Wings, Small 8(16) (2012) 2489-2494.
[19] A. Azari, S. Nikzad, The evolution of rapid prototyping in dentistry: a review, Rapid Prototyping Journal 15(3) (2009) 216-225.
[20] Q. Hamid, J. Snyder, C. Wang, M. Timmer, J. Hammer, S. Guceri, W. Sun, Fabrication of three-dimensional scaffolds using precision extrusion deposition with an assisted cooling device, Biofabrication 3(3) (2011).
[21] M.E. Hoque, Y.L. Chuan, I. Pashby, Extrusion based rapid prototyping technique: an advanced platform for tissue engineering scaffold fabrication, Biopolymers 97(2) (2012) 83-93.
[22] Y.F. Liu, X.T. Dong, F.D. Zhu, Overview of Rapid Prototyping for Fabrication of Bone Tissue Engineering Scaffold, in: G.Z. Chai, C.D. Lu, D.H. Wen (Eds.), Digital Design and Manufacturing Technology, Pts 1 and 22010, pp. 550-554.
[23] F. Rengier, A. Mehndiratta, H. von Tengg-Kobligk, C.M. Zechmann, R. Unterhinninghofen, H.-U. Kauczor, F.L. Giesel, 3D printing based on imaging data: review of medical applications, International journal of computer assisted radiology and surgery 5(4) (2010) 335-341.
[24] P. Webb, A review of rapid prototyping (RP) techniques in the medical and biomedical sector, Journal of Medical Engineering & Technology 24(4) (2000) 149-153.
[25] N.W. Choi, M. Cabodi, B. Held, J.P. Gleghorn, L.J. Bonassar, A.D. Stroock, Microfluidic scaffolds for tissue engineering, Nature materials 6(11) (2007) 908-915.
[26] N.E. Fedorovich, J. Alblas, W.E. Hennink, F.C. Öner, W.J. Dhert, Organ printing: the future of bone regeneration?, Trends in biotechnology 29(12) (2011) 601-606.
[27] S.C. Cox, J.A. Thornby, G.J. Gibbons, M.A. Williams, K.K. Mallick, 3D printing of porous hydroxyapatite scaffolds intended for use in bone tissue engineering applications, Materials Science & Engineering C-Materials for Biological Applications 47 (2015) 237-247.
[28] M. McGurk, A. Amis, P. Potamianos, N. Goodger, Rapid prototyping techniques for anatomical modelling in medicine, Annals of the Royal College of Surgeons of England 79(3) (1997) 169.

[29] S.N. Kurenov, C. Ionita, D. Sammons, T.L. Demmy, Three-dimensional printing to facilitate anatomic study, device development, simulation, and planning in thoracic surgery, The Journal of thoracic and cardiovascular surgery 149(4) (2015) 973-979. e1.
[30] A. Zhang, H. Bai, L. Li, Breath Figure: A Nature-Inspired Preparation Method for Ordered Porous Films, Chemical Reviews 115(18) (2015) 9801-9868.
[31] A. Muñoz-Bonilla, M. Fernández-García, J. Rodríguez-Hernández, Towards hierarchically ordered functional porous polymeric surfaces prepared by the breath figures approach, Progress in Polymer Science 39(3) (2014) 510-554.
[32] P. Escalé, L. Rubatat, L. Billon, M. Save, Recent advances in honeycomb-structured porous polymer films prepared via breath figures, European Polymer Journal 48(6) (2012) 1001-1025.
[33] I. Martín-Fabiani, S. Riedel, D.R. Rueda, J. Siegel, J. Boneberg, T.A. Ezquerra, A. Nogales, Micro-and submicrostructuring thin polymer films with two and three-beam single pulse laser interference lithography, Langmuir 30(29) (2014) 8973-8979.
[34] J. Rodríguez-Hernández, C. Drummond, Polymer Surfaces in Motion: Unconventional Patterning Methods, Springer2015.
[35] T.T.N. Nguyen, M.H. Luong, M.T. Do, D.M. Kieu, Q. Li, D.T.T. Nguyen, Q.C. Tong, I. Ledoux-Rak, N.D. Lai, Micro and nanostructuration of polymer materials and applications, SPIE NanoScience+ Engineering, International Society for Optics and Photonics, 2014, pp. 91710O-91710O-7.
[36] A. Michels, P. Soave, J. Nardi, P. Jardim, S. Teixeira, D. Weibel, F. Horowitz, Adjustable,(super) hydrophobicity by e-beam deposition of nanostructured PTFE on textured silicon surfaces, Journal of Materials Science 51(3) (2016) 1316-1323.
[37] L.A. Connal, R. Vestberg, P.A. Gurr, C.J. Hawker, G.G. Qiao, Patterning on nonplanar substrates: flexible honeycomb films from a range of self-assembling star copolymers, Langmuir 24(2) (2008) 556-562.
[38] H. Bai, C. Du, A. Zhang, L. Li, Breath figure arrays: unconventional fabrications, functionalizations, and applications, Angewandte Chemie International Edition 52(47) (2013) 12240-12255.
[39] J. Ding, J. Gong, H. Bai, L. Li, Y. Zhong, Z. Ma, V. Svrcek, Constructing honeycomb micropatterns on nonplanar substrates with high glass transition temperature polymers, Journal of colloid and interface science 380(1) (2012) 99-104.
[40] L. Li, Y. Zhong, J. Gong, J. Li, C. Chen, B. Zeng, Z. Ma, Constructing robust 3-dimensionally conformal micropatterns: vulcanization of honeycomb structured polymeric films, Soft Matter 7(2) (2011) 546-552.
[41] A.S. de León, A. del Campo, A.L. Cortajarena, M. Fernández-García, A. Muñoz-Bonilla, J. Rodríguez-Hernández, Formation of Multigradient Porous Surfaces for Selective Bacterial Entrapment, Biomacromolecules 15(9) (2014) 3338-3348.
[42] G. Gratzl, C. Paulik, S. Hild, J.P. Guggenbichler, M. Lackner, Antimicrobial activity of poly(acrylic acid) block copolymers, Materials Science and Engineering: C 38 (2014) 94-100.
[43] G. Lu, D. Wu, R. Fu, Studies on the synthesis and antibacterial activities of polymeric quaternary ammonium salts from dimethylaminoethyl methacrylate, Reactive and Functional Polymers 67(4) (2007) 355-366.
[44] U.H.F. Bunz, Breath figures as a dynamic templating method for polymers and nanomaterials, Advanced Materials 18(8) (2006) 973-989.
[45] M. Hernández-Guerrero, M.H. Stenzel, Honeycomb structured polymer films via breath figures, Polymer Chemistry 3(3) (2012) 563-577.
[46] M. Srinivasarao, D. Collings, A. Philips, S. Patel, Three-dimensionally ordered array of air bubbles in a polymer film, Science 292(5514) (2001) 79-83.
[47] E. Martínez-Campos, T. Elzein, A. Bejjani, M.J. García-Granda, A. Santos-Coquillat, V. Ramos, A. Muñoz-Bonilla, J. Rodríguez-Hernández, Toward Cell Selective Surfaces: Cell Adhesion and Proliferation on Breath Figures with Antifouling Surface Chemistry, ACS Applied Materials & Interfaces 8(10) (2016) 6344-6353.